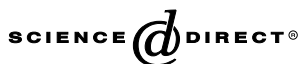


Available online at www.sciencedirect.com

Vision Research xxx (2005) xxx–xxx

**Vision
Research**

www.elsevier.com/locate/visres

Excitation mapping with the organic cation AGB²⁺

Robert E. Marc^{a,*}, Michael Kalloniatis^b, Bryan W. Jones^a

^a John A. Moran Eye Center, 50 N Medical Drive, University of Utah School of Medicine, Salt Lake City, UT 84132, USA

^b The Retinal Networks Laboratory, Department of Optometry and Vision Science, The University of Auckland, New Zealand

Received 16 June 2005; received in revised form 22 July 2005

8 Abstract

9 Excitation mapping is a method of visualizing the signaling history of neurons with permeant organic cations. It is compatible
10 with high-resolution imaging, allowing concurrent visualization of all neuronal classes and their glutamate-gated excitation histo-
11 ries. Excitation mapping documents the stability and precision of neuronal signaling *within* a given neuronal class, arguing that sin-
12 gle unit electrophysiological sampling accurately reflects neuronal diversity. We here review the theory of excitation mapping,
13 provide methods and protocol links; outline imaging concepts; provide parametric data on the temporal range and physiological
14 sensitivity of excitation mapping; and show that immunocytochemical methods for macromolecules are compatible with excitation
15 mapping.

16 © 2005 Elsevier Ltd. All rights reserved.

17 *Keywords:* Glutamate receptors; Immunocytochemistry; 1-Amino-4-guanidobutane; Agmatine; Imaging; Excitation mapping

19 1. Introduction

20 1.1. The theory of excitation mapping

21 Visualizing detailed maps of neuronal excitation is
22 motivated by the complexity of vertebrate information
23 processing assemblies such as the retina and hippocam-
24 pus, where it is difficult to confidently assign physiolog-
25 ical roles to morphologic classes of cells and more
26 difficult to predict the behavior of neuronal populations.
27 Further, electrophysiological profiling is complicated by
28 non-uniform sampling, non-stationary behavior, and
29 the high diversity of neuronal classes. Can an indepen-
30 dent method be devised to corroborate this profiling?
31 Imaging clearly offers better sampling, but what should
32 be imaged and how can it be reconciled with single unit
33 data? Older visualization methods such as radiolabeled

2-deoxyglucose transport autoradiography (described 34
in Sokoloff et al., 1977) never achieved much success 35
in retina due to poor resolution, prolonged analysis 36
times, expense, and biohazards. Newer tools such as 37
functional magnetic resonance imaging and calcium 38
imaging still suffer from extremely poor spatial resolu- 39
tion, poor coverage, incompatibility with molecular 40
markers for neuronal structure, or all three. Even when 41
calcium imaging resolution is high, sample areas and 42
depth-of-field become miniscule. Despite these limita- 43
tions, calcium signals more directly reflect immediate 44
synaptic activity than sugar transport because they often 45
represent either ligand- or voltage-gated permeation 46
events. 47

Following this line of thinking, other molecular spe- 48
cies such as organic cations can also serve as permeation 49
reporters. Tracking neuronal activity with organic cat- 50
ions is based on four basic concepts. 51

- Neurons decode and encode signals as ion currents 52
through channels 53
- Channel permeation events generate large fluxes 54

* Corresponding author. Tel.: +1 801 585 6500; fax: +1 801 581 3357.

E-mail address: robert.marc@hsc.utah.edu (R.E. Marc).

- 55 • Many key cation channels are permeated by small
56 organic reporter ions
57 • Small molecules can be haptentized to produce immu-
58 nodetection reagents

59
60 If we employ organic cations reporters and channels
61 as reporter conduits, ~~but~~ will such signals be detectable
62 in the primary fast signaling channels or “vertical” path-
63 ways of the retina served by ionotropic glutamate recep-
64 tors (iGluRs) or metabotropic mGluR6 receptors? More
65 specifically, since immunochemical detection methods
66 for small molecules routinely span ≈ 0.1 –10 mM (Marc,
67 Murry, & Basinger, 1995), how quickly will permeant
68 organic cations reach this range? Let us make the fol-
69 lowing simple but reasonable assumptions (see Hille,
70 2001 for an overview of concepts):

- 71 • A cubic cell with 10 μm edges and a volume of 1 pL
72 • A gated channel that transfers 10^6 ions s^{-1}
73 • An extracellular total permeant ion source of
74 ≈ 150 mM
75 • An extracellular reporter ion representing 3% of the
76 ion source (4.5 mM)
77 • A reporter permeation efficiency ≈ 0.4
78 • Complete probe trapping and no change in reversal
79 potential

80
81 Under these conditions, it is simple to calculate that
82 ≈ 830 channels are needed to raise the intracellular
83 reporter level from 0 to 10 mM in 10 min. Assuming
84 that glutamate receptor channel density is similar to nic-
85 otinic acetylcholine receptors, i.e., $10^4 \mu\text{m}^{-2}$ (Famb-
86 rough & Hartzell, 1972; Kunkel, Lee, & Stollberg,
87 2001), only a small fraction of the surface ($\approx 0.08 \mu\text{m}^2$
88 or 0.013%) would be required for permeation. Consider-
89 ing the small size of retinal bipolar cell dendrites, where
90 the receptor patch at a single contact might be only
91 $\approx 0.01 \mu\text{m}^2$, eight active synapses would be sufficient.
92 Thus, accumulation of immunodetectable levels of a
93 reporter molecule is predicted by the basic attributes
94 of known channels. Consistent with this, we will show
95 that both exogenous and endogenous activation of
96 iGluR channels are detectable and that there is a wide
97 tradeoff between time and reporter concentration.

98 1.2. The reporters

99 Guanidinium ions and guanidinium analogues are a
100 well-established family of organic channel permeant cat-
101 ions (Balasubramanian, Lynch, & Barry, 1995; Dwyer,
102 Adams, & Hille, 1980; Larramendi, Lorente de No, &
103 Vidal, 1956; Tasaki, Watanabe, & Singer, 1966). Their
104 permeation is based on a very compact, resonance-stabi-
105 lized cation: $\text{C}^+(\text{NH}_2)_3$. In the case of $\text{R-C}^+(\text{NH}_2)_2$
106 derivatives, efficient aldehyde trapping and hapten con-
107 jugation can be achieved if the R group contains reactive

amino groups. Fig. 1 illustrates the atomic dimensions 108
of hydrated sodium ions (Datta & Iyengar, 1991), the 109
guanidinium cation (GU), 1-amino-4-guanidobutane 110
(AGB or agmatine, the natural decarboxylation product 111
of arginine), and L-2-amino-5-guanidino-pentanoate 112
(ARG, arginine itself). 113

At physiological pH, AGB is a divalent cation due to 114
its separately protonated guanidine and amino groups, 115
while arginine is a *net* monovalent cation due to its addi- 116
tional carboxylate group. AGB likely behaves as a 117
monovalent species in terms of initial microscopic chan- 118
nel interactions with the guanidinium head, but a diva- 119
lent species in terms of macroscopic charge transfer. 120
AGB is produced at extremely low levels in the mamma- 121
lian nervous system and non-quantitative fluorescence 122
imaging suggests that most of it is associated with very 123
sparse neuronal terminals in cortex and spinal cord 124
(Fairbanks et al., 2000). Indeed, there is a large litera- 125
ture on agmatine (AGB) as an endogenous imidazole 126
receptor agonist (e.g., Raasch, Schafer, Chun, & 127
Dominiak, 2001) and anti-inflammatory agent (Fair- 128
banks et al., 2000), but the levels associated with these 129
functions are clearly far below the millimolar values 130
used in our flux experiments (see discussion in Marc, 131
1999b). On theoretical grounds at least, aldehyde- 132
trapped intracellular guanidines should be quantitative 133
reporters of time-integrated neuronal cation currents. 134
This dependence on and compatibility with glutaralde- 135
hyde cross-linking in particular means that guanidine 136
reporters could potentially provide high spatial resolu- 137
tion. If guanidine fluxes are predominantly coupled to 138
signaling processes through neuronal depolarization, 139
we can provisionally refer to such reporter detection as 140
an *excitation history*. 141

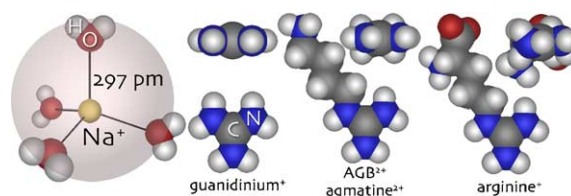


Fig. 1. Comparative sizes of guanidines and solvated Na ions. We assume a Pauling ionic radius of 97 pm for Na, a tetrahedrally bonded shell of four water molecules with Na-O bond lengths of 297 pm and H-O lengths of 99 pm. The series of guanidinium, 1-amino-4-guanidobutane (agmatine or AGB) and L-2-amino-5-guanidino-pentanoate (arginine) represents permeant species of increasing dimensions, but all are smaller or similar to the solvated Na ion in size. Each cation is shown in its largest and smallest rotational profile. Molecule shapes were generated as SMILES strings (see Weininger et al., 1989; also see Table 1 and www.daylight.com/smiles/f_smiles.html), translated to Brookhaven Protein Data Bank *.pdb format using the CORINA resource (www2.chemie.uni-erlangen.de/software/corina/index.html) and rendered with iMol v0.30 (www.pirx.com/imol).

142 1.3. Reporter detection

143 Guanidine flux visualization was first realized by
 144 Yoshikami (1981) by autoradiography of acetylcho-
 145 line-gated [³H]-AGB accumulation in frog sympathetic
 146 ganglion cells. This slow and demanding analytical
 147 method unfortunately hindered the exploration of
 148 organic cations as probes. An alternative strategy is
 149 immunodetection (Marc, 1999b). The tracking of small
 150 molecules with stereo- and regiospecific immunoglobu-
 151 lin G (IgG) reagents developed by Landsteiner (1945)
 152 has been exploited to a high degree of specificity by
 153 many laboratories. Most varieties of molecules can be
 154 haptenized and selective IgG production has been in-
 155 duced by haptens as exotic as C60 fullerenes (Chen,
 156 Wilson, Das, Coughlin, & Erlanger, 1998), as hydropho-
 157 bic as steroids (Izhaky & Pecht, 1998), and as small as
 158 glycine (Yingcharoen, Rinvik, Storm-Mathisen, &
 159 Ottersen, 1989). Thus, it is of no surprise that molecules
 160 such as AGB and ARG elicit immune responses with
 161 high selectivity. Most importantly, immunodetection
 162 can track both exogenous and endogenous molecular
 163 signals at high spatial resolution.

164 The initial strategy of these experiments is simply
 165 incubation of isolated neural tissue (retina, in this case)
 166 for brief periods in physiological media containing AGB
 167 and selective activation of iGluRs by pharmacologic
 168 agents (Fig. 2). AGB influx is proportional to the chan-
 169 nel permeability, AGB concentration and the driving
 170 force on the channel. As AGB is simply another cation
 171 in the stream, but is not extruded by Na-K ATPase, it
 172 continually accumulates. Because AGB is simply a per-
 173 meant probe, it measures current through channels over
 174 time, not voltage over time. This means that it cannot
 175 directly report the integration of excitation and inhibi-
 176 tion converging on a given cell. Indeed, converging
 177 inhibitory events that hyperpolarize the cell may in-
 178 crease the driving potential on the cation channel, slight-
 179 ly increasing the AGB current. This is an important
 180 point: AGB signaling reports an *excitation history* experi-
 181 enced by a cell due to flux through cation channels;
 182 this flux is not the summed excitation and inhibition
 183 voltages in that cell. This enables two kinds of experi-
 184 ments: (1) exogenous ligand application and (2) endoge-
 185 nous modulation of glutamate release. In this review, we
 186 will illustrate how to tune AGB concentration and expo-
 187 sure time to preferentially detect only large signals such
 188 as direct exogenous activation of AGB permeation or to
 189 sensitively report endogenous glutamate-gated perme-
 190 ation events. In the latter, endogenous glutamate release
 191 from bipolar cells onto amacrine and ganglion cells is
 192 controlled by integrated excitation and inhibition. As
 193 AGB signals only report permeation through gluta-
 194 mate-activated channels, this means that downstream
 195 AGB signals in ganglion cells include a presynaptic or
 196 upstream *network history* (Fig. 2). Postsynaptic inhibi-

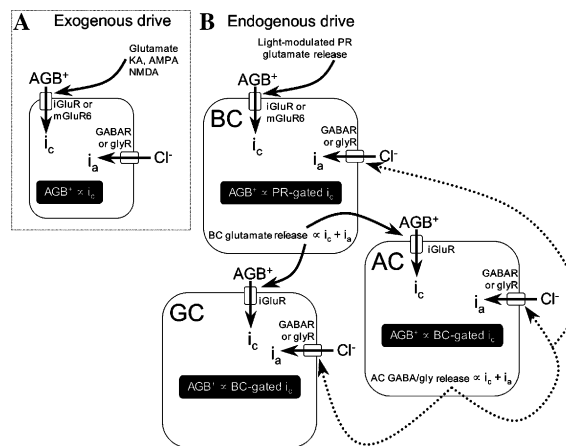


Fig. 2. AGB reporter schemes to detect (A) exogenous ligand-gated and (B) endogenous glutamate-gated cation currents in neurons. (A) Exogenous drive: a range of exogenous ligands activates cation-permeant iGluR or mGluR6 channels (KA, kainate; AMPA, α -amino-3-hydroxy-5-methylisoxazole-4-propionic acid; NMDA, *N*-methyl-D-aspartate). Using a protocol shown to be insensitive to endogenous signals (5 mM AGB, 10 min incubations, Marc, 1999b), AGB signals are proportional to the total iGluR or mGluR cation currents (i_c). Anion currents (i_a) mediated by GABA and glycine receptors (GABAR, glyR) do not reduce this signal and may slightly increase it by increasing the driving force. (B) Endogenous drive: photoreceptor (PR) \rightarrow bipolar cell (BC) \rightarrow amacrine and ganglion cell (AC,GC) signaling chains depend on intrinsic glutamate release from either PRs or BCs. This can be detected by increasing incubation time or AGB concentration. Glutamate released by photoreceptors modulates AGB permeation into BCs. However, i_c and i_a (and other mechanisms) antagonistically sum to control release of glutamate from BCs, so that the AGB signal in ACs and GCs, in particular, reports the sum of presynaptic excitation and inhibition via glutamate release from BCs.

tion directly on the ganglion cell itself is undetected by
 AGB permeation, so the endogenous mapping method
 theoretically has the potential to segregate the effects
 of presynaptic amacrine cell \rightarrow bipolar cell feedback
 from postsynaptic amacrine cell \rightarrow ganglion cell
 feedforward.

2. Methods

2.1. The reporters

AGB is commercially available as a sulfate salt
 (1-amino-4-guanidobutane, $C_5H_{14}N_4 \cdot H_2SO_4$, CAS
 2482-00-0) from Sigma-Aldrich and Fluka at 97–99%
 purity. The major contaminant is usually arginine,
 which is of no permeation consequence at low cation
 fractions. Similarly, brief elevations of sulfates to 3–
 10 mM appears to be of little physiological consequence
 (Marc, 1999b). However, longer exposures or higher
 AGB sulfate concentrations may be physiologically
 unacceptable, leading to partial anion channel block
 and failure of osmotic regulatory volume control
 (Petrunikina, Harrison, Ekhlasi-Hundrieser, &

217 Töpfer-Petersen, 2004). A biionic solution of pure AGB
 218 sulfate thus triggers instability of horizontal cell mem-
 219 brane potentials, and this is corrected by using AGB
 220 chloride (Marc, Lembke, Solessio, & Rapp, unpublished
 221 data). AGB chloride is not commercially available but
 222 can be produced in the laboratory at reasonably high
 223 purity using either arginine decarboxylation at small-
 224 scales or BaCl₂ precipitation at large scales (Marc,
 225 unpublished data; see <http://prometheus.med.utah.edu/~marclab/agb.html>). AGB is normally stored at
 227 –20 °C, but we have found no evidence of degradation
 228 at least up to 30 days dry and 7 days aqueous solution
 229 storage at 4 °C. ARG, D-arginine (dARG) and guanidi-
 230 nium (GU) are commercially available as free acids or
 231 chloride salts. Saline solutions containing AGB, ARG,
 232 dARG or GU are made by adding the guanidines imme-
 233 diately before use without NaCl replacement for concen-
 234 trations ≤5 mM and with NaCl replacement otherwise.
 235 Guanidines are compatible with Hepes buffer and stan-
 236 dard bicarbonate buffering; we have not evaluated Tris
 237 but do not recommend it. As shown in Table 1, the
 238 guanidinium groups of AGB, ARG, and dARG are cations
 239 at physiological pH (Gründemann, Hahne, Berkels,
 240 & Schömig, 2003; e.g., pK_a for the guanidine in argi-
 241 nine = 12.5). The primary amine has only a slightly low-
 242 er pK_a (arginine and AGB pK_{a2} ≈ 9) and, consequently,
 243 these molecules are net cations at physiological pH
 244 (AGB²⁺, ARG⁺, dARG⁺). The data presented in this
 245 paper deal exclusively with AGB²⁺ detection.

246 2.2. The detectors

247 Rabbit polyclonal IgGs targeting AGB, ~~R~~, ~~dR~~, and
 248 GU were produced using BSA–glutaraldehyde–amine
 249 conjugate immunogens (described in Marc et al.,
 250 1995). Anti-AGB IgGs licensed to Signature Immunolo-

251 gics (Salt Lake City, UT) are distributed by Chemicon
 252 International (Temecula, CA). Samples of any of these
 253 are available upon request from the Marc Laboratory
 254 at the University of Utah. These reagents are stored at
 255 –70 °C in serum and are stable indefinitely at 4 °C in
 256 a 100× concentrate working solution in 0.1 M phosphate
 257 buffer, pH 7.4, with 1% lyophilized goat serum as a pro-
 258 tein carrier and 0.05% thimerosal. Full working solu-
 259 tions are stable for over 1 year at 4 °C. Anti-agmatine
 260 IgG have also been produced by the Reis laboratory
 261 (e.g., Fairbanks et al., 2000) at Weil-Cornell Medical
 262 College, NY. We have not evaluated them but presume
 263 them to behave similarly.

264 2.3. Tissue preparation and exposure

265 AGB in particular has been used in vitro for several
 266 tissue systems or in vivo via intravitreal injections for
 267 retinal mapping and aqueous exposure for fish olfactory
 268 system mapping (Edwards & Michel, 2002, 2003; Lips-
 269 chitz & Michel, 2002; Sakata, Olson, & Michel, 2003).
 270 The in vitro protocol for retina has been described in de-
 271 tail (Marc, 1999a; Marc, 1999b) but involves mounting
 272 isolated retinal pieces ganglion-cell side down on cellu-
 273 lose triacetate filters as a support during tissue handling.
 274 A key strategy for performing incubations derives from
 275 our long experience with autoradiographic mapping of
 276 radiolabeled ligand transport and involves razor cutting
 277 filter-mounted retinas into small pieces prior to incuba-
 278 tion, optimizing tissue use. Cut edges can evoke artifac-
 279 tual AGB signals (Marc, 1999b) as many retinal neurons
 280 and horizontal cells in particular are strongly coupled by
 281 gap junctions permeant to small molecules such as AGB
 282 or ARG. It is important to age cut pieces for 3–5 min in
 283 oxygenated, warm solutions to allow the cells to heal.
 284 Neural tissue must be also be handled with great care

Table 1
Cation channel reporters

Name	Code	IUPAC	Formula	Canonical SMILES (*isomeric)
Guanidinium ⁺ MW 60.079 CID 32838 pK _a 12.6	GU	Diaminomethylideneammonium	CH ₆ N ₃	C(=N)(N)N
L-Arginine ⁺ MW 174.201 CID 232 pK _{a1} 12.5 pK _{a2} 9	ARG	L-2-Amino-5-guanidino-pentanoate	C ₆ H ₁₄ N ₄ O ₂	C(CC(C(=O)O)N)CN=C(N)N
D-Arginine ⁺ MW 174.201 CID 7170 pK _a values assumed same as L-arginine	dARG	D-2-Amino-5-guanidino-pentanoate	C ₆ H ₁₄ N ₄ O ₂	*C[C=C=H](C(=O)O)N)CN=C(N)N
Agmatine ²⁺ MW 130.192 CID 199 pK _{a1} 12.5 pK _{a2} 9	AGB	4-Aminobutyliminomethanedi-amine also 1-amino-4-guanidinobutane	C ₅ H ₁₄ N ₄	C(CCN=C(N)N)CN

285 as guanidines present at immunodetectable extracellular
 286 levels can become fixed to the protein matrix of dam-
 287 aged cells (e.g., rods with broken outer segments) and
 288 can permeate glial cells that respond to local damage
 289 by activation of non-selective stretch sensitive cation
 290 channels (Marc, 1999b). Excitation mapping with guan-
 291 idinium analogues thus reports all anomalies of tissue
 292 handing. Mouse tissues in particular are extremely sen-
 293 sitive and tissue handling or ligand-induced swelling
 294 can activate significant permeation into Müller cells
 295 (Rohrer et al., 2004). Labeling of broken cells could be
 296 reduced by rinsing prior to fixation, but this increases
 297 the chance of breaking more rods or stretch-activating
 298 MCs. Labeling of ruptured cells might be cleared by
 299 washing, but we argue that it is advantageous to clearly
 300 report the state of all cells.

301 Salines containing guanidinium analogues as report-
 302 ers are inexpensive, so large numbers of samples or large
 303 retinal pieces are easily accommodated. Our routine
 304 method involves transferring each piece from its holding
 305 medium to small droplets (0.1–0.25 ml) of test medium
 306 containing activating ligands, antagonists, competitors,
 307 and reporters. Each piece is slipped into the droplet
 308 from the side, grasping only the filter with fine forceps,
 309 and an array of pieces concurrently incubated in a
 310 60 ml disposable polystyrene dish with a loose cover
 311 continuous gas flow (95% O₂/5% CO₂) with bicarbon-
 312 ate-based Ames and 100% O₂ with Hepes Ames. The
 313 Kalloniatis laboratory uses Edwards medium (Edwards,
 314 Konnerth, Sakmann, & Takahashi, 1989) for rodent
 315 work. Immediately after incubation, fixative may be
 316 added directly to the droplets so that the tissues are
 317 well-stabilized before handling. Free amino acid and
 318 reporter signal trapping in isolated retinal samples is
 319 complete by 10 min using a standard 250 mM (2.5%)
 320 glutaraldehyde, 333 mM formaldehyde (1%) fixative
 321 (Marc, unpublished data).

322 2.4. Time and concentration

323 As originally shown in Marc (1999b), the accumula-
 324 tion of AGB at short times and high concentrations is
 325 not due to transporter activity, but rather channel per-
 326 meation. Consequently, incubation time and AGB con-
 327 centration should be inversely related over a wide range.
 328 The original selection of a basal 5 mM AGB level and
 329 10 min incubation was motivated by the intent to track
 330 pharmacologically gated permeation events and these
 331 conditions were found to avoid significant endogenous
 332 signals. Raising the concentration to 25–50 mM confers
 333 greater sensitivity by increasing the fractional flux and it
 334 is possible to obtain strong signals in 60–120 s of AGB
 335 exposure in vitro. A key difference between exogenous
 336 ligand activated and endogenous glutamate signaling is
 337 the weaker efficacy of glutamate compared to kainate,
 338 AMPA, and NMDA. Increasing the concentration of

339 AGB to 25 mM and/or the exposure time to 20 min thus
 340 amplifies detection by 2- to 10-fold in terms of net flux.
 341 As we will show, this enables detection of endogenous
 342 rod and cone activated signaling, as well as permeation
 343 through mGluR6-gated channels (also see Kalloniatis,
 344 Sun, Foster, Haverkamp, & Wässle, 2004). The ability
 345 to exchange time and concentration in the 1–100 mM
 346 range eliminates transporters as potential contributors
 347 to the flux signal (Gründemann et al., 2003; Marc,
 348 1999b).

349 2.5. Fixation

350 The key to quantitative analysis of signaling with
 351 reporters is high-efficiency trapping and the dialdehyde
 352 fixative glutaraldehyde is ideal for both AGB trapping
 353 and visualization of small molecule signatures. While
 354 the routine trapping medium for AGB and small mole-
 355 cules is a variant of Karnovsky's medium, any properly
 356 buffered fixative with an appropriate level (10–250 mM)
 357 of glutaraldehyde will trap >85% of all endogenous
 358 amines. This is due to the dendrimer-like reactions that
 359 most amines generate with glutaraldehyde as a core, and
 360 trapping runs until all amines are exhausted (see [http://
 361 prometheus.med.utah.edu/~marclab/CMP_sub-
 362 strates.html](http://prometheus.med.utah.edu/~marclab/CMP_substrates.html)). It is very important to include the monoal-
 363 dehyde formaldehyde at 100–1000 mM, so that most of
 364 the matrix sites in tissue are decorated with a complex
 365 surface of large and small aldehyde links. This tremen-
 366 dously decreases background binding of IgGs. In gener-
 367 al, we use: 250 mM glutaraldehyde (2.5%), 333 mM
 368 (1%) formaldehyde, 1 mM MgSO₄, and 3% sucrose in
 369 100 mM phosphate buffer at pH 7.4. This fixative is
 370 incompatible with most IgGs targeting macromolecules.
 371 Kalloniatis and colleagues have shown that it is possible
 372 to use 1 mM (0.01%) glutaraldehyde (1 with 1332 mM
 373 4%) formaldehyde and fluorescence detection to visual-
 374 ize AGB permeation and characteristic protein markers
 375 concurrently.

376 2.6. Sample preparation and visualization

377 Our ~~CMP visualization~~ technologies (Marc & Camer-
 378 on, 2002) are based on thin section methods, which re-
 379 quire resin-based embedding to achieve reliable thin
 380 200–40 nm ultrathin serial sections. After fixation, tis-
 381 sues are dehydrated in graded methanols to acetone,
 382 infiltrated with epoxide resins and cured into blocs hard
 383 enough for electron beam stability but soft enough for
 384 thick section remounting methods. As retinas can be
 385 embedded as flat sheets, stacks of retinas can be assem-
 386 bled into sample arrays where a single thin section can
 387 contain samples from 1 to 10 experiments (Marc,
 388 1999b; Marc, Liu, Kalloniatis, Raiguel, & van Hae-
 389 sendonck, 1990). Complete protocols for both resin
 390 embedding and stack fabrication are available at

insert "(see below)"

insert "computational molecular phenotyping (CMP)"

391 <http://prometheus.med.utah.edu/~marclab/protocols.html>. Samples are sectioned into serial arrays on 12-
392 well HTC slides (Erie Scientific) for concurrent probing
393 for a *basis set* of small molecules, including L-alanine
394 (A), L-aspartate (D), L-glutamate (E), glycine (G), gluta-
395 thione (J), L-glutamine (Q), taurine (τ), and GABA (γ , γ -
396 aminobutyric acid): A · D · E · G · J · Q · τ · γ . This basis
397 set is augmented by the excitation reporter AGB (B).
398

399 Probed CMP datasets are visualized with silver inten-
400 sification, providing archival quantitative imagery (Kal-
401 loniatis & Fletcher, 1993; Kalloniatis, Marc, & Murry,
402 1996; Marc et al., 1990). Detailed protocols are available
403 at the Marc laboratory web site, <http://prometheus.med.utah.edu/~marclab/protocols.html> along
404 with descriptions of surface detection methods ([http://prometheus.med.utah.edu/~marclab/CMP_sub-](http://prometheus.med.utah.edu/~marclab/CMP_substrates.html)
405 [strates.html](http://prometheus.med.utah.edu/~marclab/CMP_substrates.html)). Thin section images not previously pub-
406 lished were captured at a calculated pixel scaling of
407 182 nm/pixel (40 \times planapochromatic oil immersion lens)
408 with a QImaging QICAM IEEE-1394 12-bit cooled
409 monochrome camera (www.qimaging.com) operated in
410 the 8-bit mode. Illumination was controlled with a reg-
411 ulated Oriel power supply and no ripple or long-term
412 drift was detectable. All images were tiled and aligned
413 as previously described (Marc & Cameron, 2002) and
414 no filtering or contrast adjustment was used prior to im-
415 age analysis. Raw images are available at <http://prometheus.med.utah.edu/~marclab/datasets.html>.

419 Alternative methods include low glutaraldehyde-high
420 paraformaldehyde methods and cryosectioning followed
421 by double labeling with anti-AGB and other cell-specific
422 anti-macromolecule markers (see Haverkamp & Wässle,
423 2000 for protocols). The key to this method is to in-
424 crease anti-AGB concentrations about to compensate
425 for the low trapping efficiency of the fixative. This nec-
426 essarily renders AGB signaling somewhat qualitative,
427 but this is nevertheless an important advance. The major
428 protocol adjustments are AGB incubation at 25 mM,
429 fixation in 1 mM glutaraldehyde and 1332 mM parafor-
430 maldehyde, and cryoimmunocytochemistry with five times
431 higher anti-AGB IgGs.

432 2.7. CMP greyscale analysis

433 The main tools used for quantitative analysis of grey-
434 scale images are univariate histogramming and N-space
435 cluster analysis, implemented as described in Marc et al.
436 (1995) and Marc and Jones (2002). A tutorial on cluster
437 analysis is available at http://prometheus.med.utah.edu/~marclab/CMP_analysis.html. The important concept
438 underlying analysis of greyscale images is the fundamen-
439 tal trial-to-trial precision of the method across users and
440 time, and the ability of greyscale images to encode
441 roughly 2 log units of molecular concentration as pixel
442 value (Marc & Jones, 2002). Our basic tool for univari-
443 ate and multivariate histogram analysis is CellKit, an

445 application developed in the Marc laboratory under
446 the IDL image visualization language (www.rsinc.com)
447 and operates in the freely distributed IDL VM environ-
448 ment. CellKit v2.2 is available from http://prometheus.med.utah.edu/~marclab/protocols_cellkit.html.
449

450 3. Results

451 3.1. Visualizing excitation history

452 Brief incubations (≤ 10 min) in low concentrations of
453 AGB (≤ 5 mM) in the absence of any activating agent re-
454 veal no differential neuronal AGB signal in retina using
455 standard silver visualization. However, activation with
456 100 μ M KA (a saturating dose; see Marc, 1999b) is high-
457 ly effective and evokes strong AGB entry into horizontal
458 cells, bipolar cells, amacrine cells, and ganglion cells
459 (Fig. 3). Importantly, all horizontal cells of a given class
460 (e.g., type B) behave identically (Marc, 1999a, 1999b),
461 which provides a basis for understanding variation in
462

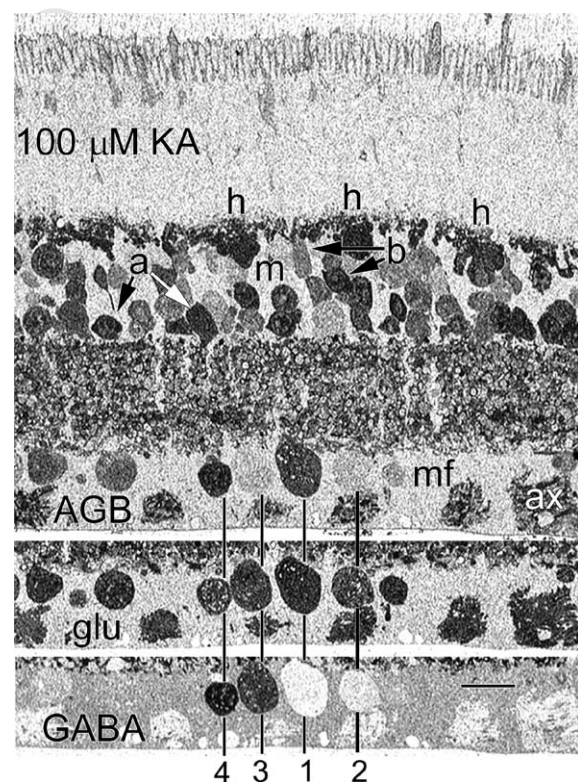


Fig. 3. AGB signals isolated in rabbit retina after incubation with 5 mM AGB + 100 μ M KA. Endogenous glutamate (glu) and GABA signals in the ganglion cell layer are shown as registered strips from serial sections with selected cell classes marked by vertical lines with labels below: 1, E+ ganglion cells with strong AGB responses; 2, E+ ganglion cells with weak signals; 3, E+/ γ + ganglion cells with weak AGB signals; 4, γ + starburst amacrine cells with strong signals. ax, Ganglion cell axon bundles, m Müller cells, mf Müller cell end feet. Amacrine (a) and bipolar (b) cells also display a range of responses while horizontal (h) cells all show the same response. Scale bar, 20 μ m. Reproduced from Marc (1999) by permission of Wiley Interscience.

insert "b"

462 signaling in more complex populations of amacrine and
 463 ganglion cells. If a single neuronal class behaves consis-
 464 tently, cells with different grey level responses are likely
 465 to be biologically different classes. As 100 μ M KA
 466 should be saturating for all AMPA receptor subtypes,
 467 the presence of cells with weak AGB signals implies that
 468 either few channels are expressed per cell or the unitary
 469 conductance of each assembly is low, or both. We dem-
 470 onstrated that this argument is consistent with the label-
 471 ing behavior of individual ganglion cell classes (Marc &
 472 Jones, 2002). The differential *concurrent* activation of
 473 different neuronal populations by a single application
 474 of an agonist can be documented by correlating multiple
 475 molecular signals from the basis set with reporter signals
 476 of individual cells in registered serial sections (Fig. 3).
 477 Specifically, γ + starburst amacrine cells and large E+
 478 ganglion cells show strong AGB signals in response to
 479 100 μ M KA, whereas certain medium-sized ganglion
 480 cells and some dual E+/ γ + ganglion cells demon-
 481 strate little or no induced response. We have shown that the
 482 latter belong to a class of ganglion cells (Marc & Jones,
 483 2002, class 12) that likely correspond to a set of sluggish
 484 transient ganglion cells. In addition, it is clear that only
 485 a subset of bipolar cells is activated by KA (Marc,
 486 1999a; Rohrer et al., 2004) and these, by definition,
 487 should be OFF bipolar cells.

488 Do polysynaptic effects confound these pharmacologic
 489 signals? While it is certain that KA-activated bipolar cells
 490 will release glutamate and must trigger permeation events
 491 via both AMPA and NMDA receptor channels in target
 492 cells, and that this additional signal should be superim-
 493 posed on the intrinsic KA-activated AMPA receptor sig-
 494 nal, can we see that increment with brief (10 min)
 495 exposures and low (5 mM) levels of AGB? Might not nic-
 496 otinic pathways corrupt the datasets? Six kinds of exper-
 497 iments reported in Marc (1999b) argue not.

- 498 (1) Endogenous glutamate signaling is not detectable
 499 with this brief protocol.
 500 (2) Exogenous glutamate signaling is not detectable
 501 without blockade of glutamate transporters (i.e.,
 502 blocking presynaptic and glial clearance of gluta-
 503 mate). Thus, it is unlikely that KA-evoked gluta-
 504 mate release could be differentially detected.
 505 (3) KA and NMDA activation generate very different
 506 laminar patterns of signaling in the inner plexiform
 507 layer. If endogenous glutamate release were a signif-
 508 icant source of AGB signal, KA stimulation should
 509 mimic NMDA response patterns. It does not.
 510 (4) NMDA antagonists do not change the KA
 511 pattern.
 512 (5) KA agonists *do* change the NMDA pattern, but
 513 only by reducing its peak value. This demonstrates
 514 that endogenous occupancy of the AMPA recep-
 515 tor is likely the key mechanism overcoming volt-
 516 age-dependent NMDA block.

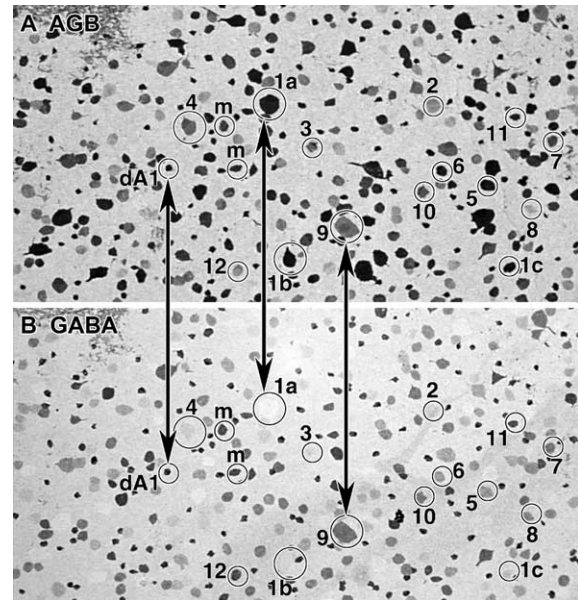


Fig. 4. Two images from a 7-dimensional molecular series through the rabbit ganglion cell layer after activation with 25 μ M AMPA. These two panels show correlated signals of 15 classes of resident neurons in the ganglion cell layer, including γ + displaced starburst amacrine cells (dA1) and 14 classes of ganglion cells. Two misplaced amacrine cells (m) are also indicated. Each image is 885 μ m in width. Excerpted from Marc and Jones (2002) by permission of the Society for Neuroscience.

insert "(A, AGB; B, GABA)"

- (6) Activation of nicotinic receptors with carbachol, epibatidine or acetylcholine does not generate any AGB signal.

Presuming the ligand-driven responses to be uncon-
 terminated by endogenous networks, it follows that re-
 sponse diversity can be exploited to discover and
 display physiological classes of neurons. By sectioning
 in the horizontal plane of of cell somas such as the
 ganglion cell layer (Fig. 4), it is possible map to concurrent
 responses of a large cohort of neurons and extract their
 molecular signatures using CMP and a basis set of
 probes. These data demonstrate that each single gangli-
 on cell class possesses a characteristic permeation re-
 sponse to AMPA receptor activation. We argue that
 this fundamental response strength is partially responsi-
 ble for the differential spiking patterns of ganglion cells:
 that cells with large responses are brisk and those with
 weak responses are sluggish variants (Marc & Jones,
 2002).

3.2. Greyscale analysis

The data in Fig. 4 provide an ideal opportunity to
 illustrate the quantitative nature of the silver-based visu-
 alization method and CMP. Concurrent univariate and
 bivariate histograms of AGB and GABA signals of gan-
 glion cell classes 1, 3, 5, and 12 are shown in Fig. 5 along
 with the entire neuronal cohort signal histograms. The

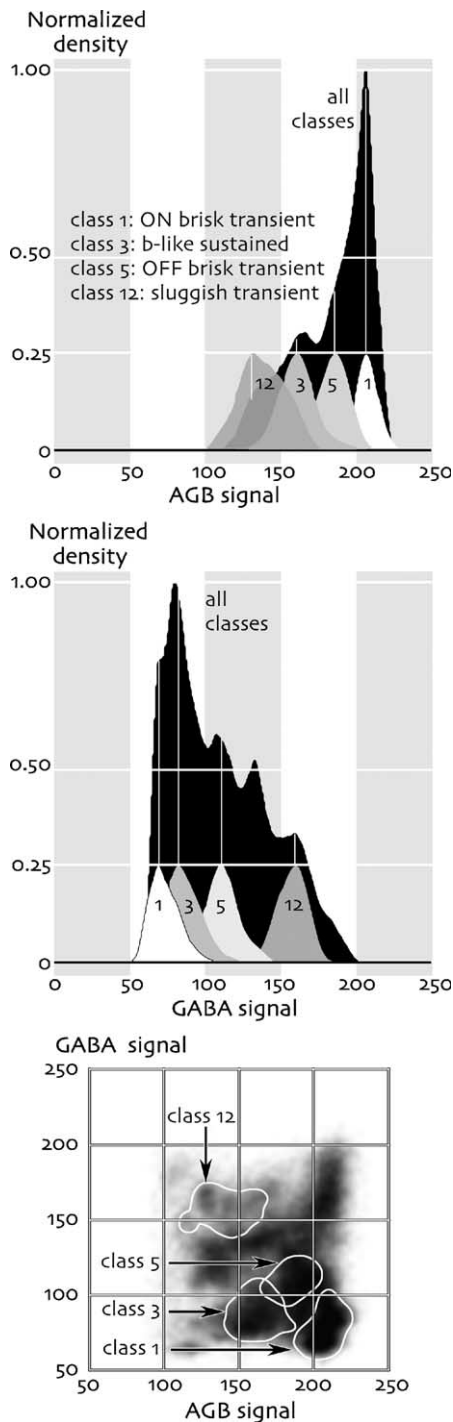


Fig. 5. Peak-normalized AGB and GABA univariate and bivariate signal strength histograms for a sample of over 600 ganglion cells. The abscissa is the 8-bit AGB or GABA grey level intensity (0–255) and the ordinate is normalized probability density. Top: the histogram for all cells in the ganglion cell layer is shown in black. The underlying histograms for classes 1, 3, 5, and 12 (see Fig. 4) are arbitrarily normalized to 0.25 to visualize their different positions along the AGB signal axis. Class 1 cells are the most AMPA-responsive. Middle: the same sets of cells visualized as histograms of GABA signals. Bottom: the same sets of cells visualized as a bivariate AGB vs GABA density histogram with the borders of the 95% level skirts of each class outlined in white. Bivariate clustering shows better separability than univariate analysis.

use of quantitative grey level immunocytochemical data allows extremely powerful segmentation of images, especially when higher dimensions of data are available. The univariate AGB signals of all four classes represent different distributions with very high significances ($p < 0.0001$ for any pair using parametric models). However, one cannot extract the classes from a single image because the distributions overlap. For example, class 12 overlaps class 3 in AGB response and class 5 overlaps 1. Similarly, classes 1, 3, and 5 overlap in GABA content. By considering their *bivariate* signals, however, it is clear that class 12 exists in a molecular space that is always separate from the other three, and that despite their univariate overlaps, classes 1, 3, and 5 each occupy a unique portion of signal space. By extending this kind of analysis to three and more molecular dimensions, further power in separability is acquired (see Marc & Jones, 2002).

3.3. Exchanging time and AGB concentration

Our initial analyses of AGB permeation at 5 mM for 10 min showed that retinal OFF bipolar cells were selectively activated by AMPA and KA; that ON bipolar cells were apparently not permeant to AGB or at least not detectable (Marc, 1999a, 1999b). By increasing either the exposure time or the concentration of however, it became clear that the non-selective cation channels of ON bipolar cells were AGB-permeant and that this endogenous signaling could be blocked by 2-amino-4-phosphonobutyrate (AP4, Kalloniatis et al., 2004). This implies that increased flux is required to detect ON bipolar cells, and that the product of the AGB permeability, unitary conductance and density channels gated of by the mGluR6 receptors is significantly smaller than for AMPA or NMDA receptors. It further argues that AGB behaves as a classic permeant cation, showing little detectable channel saturation, and is further evidence that AGB enters cells by channel permeation and not transport.

We have parametrically explored the temporal and sensitivity limits of excitation mapping. A major strength of the CMP method is the ability to stack multiple samples into a single bloc and probe them concurrently. Isolated rabbit retinal samples mounted on filter chips were incubated in parallel for varied times in different AGB concentrations while activated in 50 μ M KA and then concurrently probed as stacks. Fig. 6 shows the extent of response detection achieved at low and high concentrations. As originally described in Marc (1999a), 5 mM AGB at 10 min is a highly sensitive regime and produces extremely strong responses in all superclasses of retinal neurons. Even so, strong responses are detectable even at 2 min of incubation and the responses of the most sensitive neurons in the retina, starburst amacrine cells are evident at 60 s. One

544
545
546
547
548
549
550
551
552
553
554
555
556
557
558
559
560
561
562
563
564
565
566
567
568
569
570
571
572
573
574
575
576
577
578
579
580
581
582
583
584
585
586
587
588
589
590
591
592
593
594
595
596
597

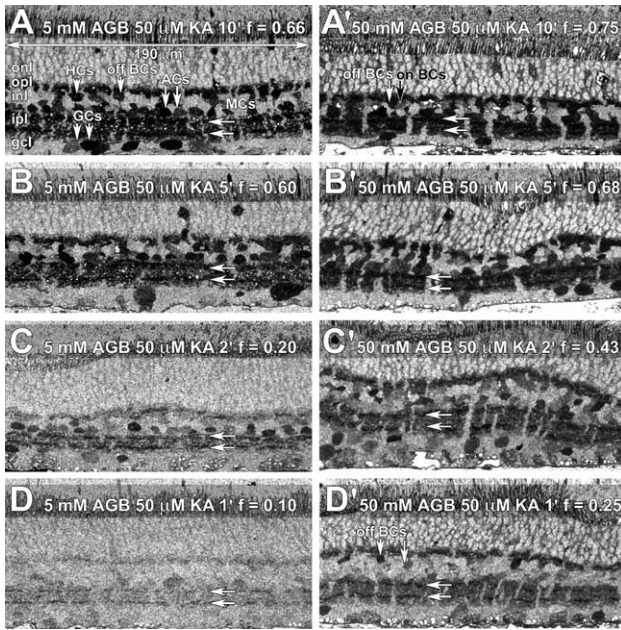


Fig. 6. The time course of AGB permeation at high and low AGB levels. (A–D) Matched retinal samples incubated under 50 μ M KA activation in 5 mM AGB for 1, 2, 5, and 10 min. (A'–D') Matched retinal samples incubated under 50 μ M KA activation in 50 mM AGB for 1, 2, 5, and 10 min. (A) Indexes responsive horizontal (HCs), OFF bipolar (off BCs), amacrine (ACs), and ganglion (GCs) cells. Müller cells (MCs) maintain the same background signal at all activation levels. Horizontal arrows mark the stratification levels of starburst amacrine cells. In each panel, the fractional response (f) of the inner plexiform layer (ipl) is shown (see Marc, 1999b for calculation). At high AGB levels (50 mM, A'), ON bipolar cells begin to show endogenous permeation in vitro. Each panel is 190 μ m wide. Other abbreviations: onl, outer nuclear layer; opl, outer plexiform layer; inl, inner nuclear layer; gcl, ganglion cell layer.

non-saturating (Figs. 7 and 8). This is consistent only with the behavior of a channel and completely excludes transporters as possible entry routes. Furthermore, it demonstrates that AGB selectively tracks excitation history over a wide range of probe levels. This sets the stage for using AGB as an in vivo probe and a probe of endogenous signaling, which we have achieved in several formats. These are beyond the scope of this review, but should encourage other investigators to explore the use

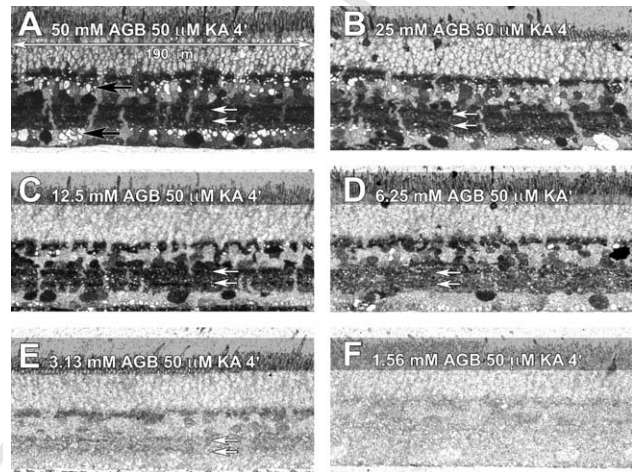


Fig. 7. The concentration-dependence of AGB permeation. A single rabbit retina was cut into chips and each concurrently incubated for 4 min in 50 μ M KA and serial 2-fold dilutions of AGB ranging from 50 to 1.56 mM. As in Fig. 6, white arrows mark the starburst amacrine strata. This sample showed some Müller cell swelling at the highest concentrations, but this is a variable effect and may be due to mechanical stimulation (see Marc, 1999b).

robust measure of retinal responsivity to pharmacologic activation is the fractional response (f) introduced in Marc (1999b). This measure is substantially different from the total greyscale signal (cf. Sun, Rait, & Kallo-niatis, 2003). The fractional response is an area measurement that asks: “What fraction of the neuropil has been activated above a specified detection threshold.” This allows direct comparison of total responsivity among retinas, even though individual cell classes have different saturation levels to a ligand. Thus, a saturating KA fractional response is in the range of 0.55–0.70 for 5 mM AGB at long times and progressively less a short times. Though this is a non-linear measure, it nevertheless demonstrates that 50 mM AGB at only 60 s generates a KA activation signal that is much greater than 5 mM can achieve in 2 min. These data show that excitation mapping has a wide latitude and that AGB concentration and time are readily exchangeable.

Importantly, the ligand activated AGB permeation into retinal neurons is an increasing function of AGB concentration and even at 50 mM AGB, representing about 1/3 of all permeant cations, the flux appears

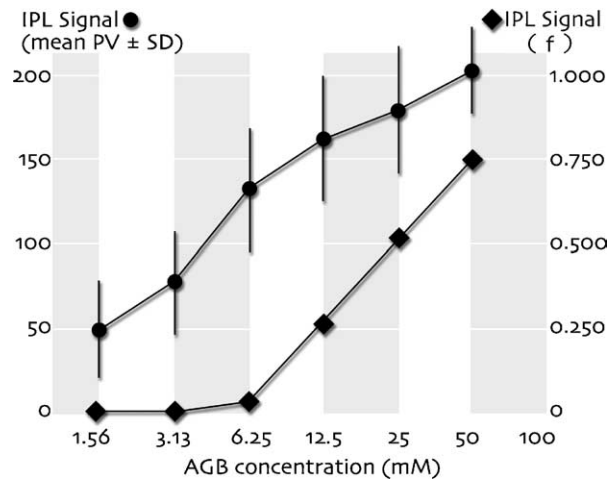


Fig. 8. Increasing grey level signal as mean pixel value (PV = dots) \pm 1 standard deviation (SD) and fractional response (f = diamonds) as a function of AGB concentration for a constant 4 min activation with 50 μ M KA. These data were abstracted from the retinas in Fig. 6 over 0.5–1 mm of length of retinal tissue, each spanning $>10^3$ retinal neurons. PV was measured as the mean histogram signal for the isolated IPL. PV is more sensitive than FR, but both show increasing flux as a function of AGB concentration, showing that the signal is consistent solely with a permeation process.

of this probe. The important message is that AGB mapping is very tolerant of diverse conditions and can be tuned to high sensitivities with high concentrations of AGB, while remaining sensitive at low concentrations that do not perturb ionic balances. Indeed, it should be emphasized that AGB use is not without risk, as it appears to be an inhibitor of Na-K ATPase through antagonism at the Na binding site (Or, David, Alla Shainskaya, Tal, & Karlshis, 1993) and is an inhibitor of NO synthase (Feng, Piletz, & LeBlanc, 2002; Galea, Regunathan, Eliopoulos, Feinstein, & Reis, 1996). But since both of these actions require AGB to permeate and accumulate to significant levels, it is likely that they play no major role in short-term response patterns.

3.4. Endogenous signal mapping

The greyscale sensitivity and enhanced detectivity with increased AGB concentration gives AGB the potential for mapping endogenous glutamate signaling, which induces much smaller signals than exogenous pharmacologic drive. But since we can increase sensitivity 2- to 3-fold by using longer incubations, carefully controlled lighting conditions routinely trigger AGB permeation in both ON and OFF bipolar cells. This response pattern is only elicited successfully in on-choroid preparations. Isolated retinas show little activity even after 20 min in 5 mM AGB. Fig. 9 shows excitation mapping in a dark-adapted on-choroid rabbit retina driven in vitro with mesopic ($1.84 \text{ quanta s}^{-1} \mu\text{m}^{-2}$) 550 nm 2 Hz^2 -wave light for 20 min in the presence of 5 mM AGB. This stimulus flux is about a log unit above threshold for most cone ON bipolar cells and a log unit below that of the least sensitive cone ON bipolar cells (see Fig. 6 in Pang, Gao, & Wu, 2004). All B-type horizontal cells are homogeneously light responsive, while each bipolar cell cohort is multimodal (Fig. 10). Rod bipolar cell light responses are not quantitatively distinguishable from those of most cone-driven OFF bipolar cells and they collectively form modes 2 and 3 of the light-response histogram. A sparse set of highly responsive bipolar cells appears give the strongest signals and form mode 1. We believe these are cone-driven OFF bipolar cells, but verifying this will require further analysis with horizontal sections. Cone-driven ON bipolar cells, identified by their glycine content (e.g., Marc, 1999a), are clearly segregated into three modes under 550 nm light: high, medium and unresponsive. It is, tempting to presume that mode 3 represents cells driven by blue cones, but that remains to be seen. Starburst amacrine cells remain the most sensitive of the inner retinal neurons. We had previously shown that they were the most responsive amacrine cell when driven by AMPA and kainate (Marc, 1999a, 1999b, Marc & Jones, 2002), but this demonstrates that they are also likely the most sensitive

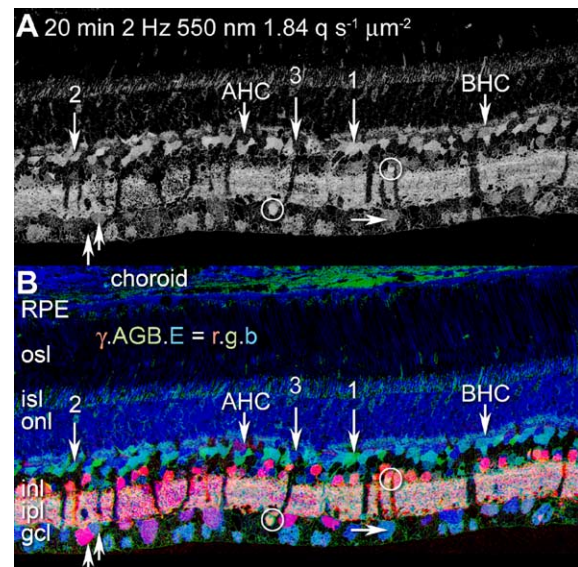


Fig. 9. Light-driven AGB signals in the in vitro rabbit retina with intact RPE and choroid. The retina was driven 20 min with $1.84 \text{ quanta s}^{-1} \mu\text{m}^{-2}$ 550 nm 2 Hz^2 -wave light (50% duty cycle) in Ames medium with 5 mM AGB. The top panel shows the AGB response alone (as an inverted, brightness-scaled image) and the bottom is a $\gamma \cdot \text{AGB} \cdot E \text{ rgb}$ mapping. Strong permeation was activated in a great range of target neurons including all rod bipolar cells, cone OFF bipolar cells and most but not all cone ON bipolar cells and not type A horizontal cells. Cell classes were defined by CMP signatures (see Marc, 1999a; Marc and Jones, 2002). Arrows denote instances of the three modes of cone ON bipolar cell responses. Mode 1 is a highly responsive cohort, mode 2 shows moderate responses and mode 3 shows no responses. ON and OFF starburst amacrine cells are circled, which have strong mesopic light responses. Ganglion cell signals were weaker and varied by class (upward arrows) with α -like cells (horizontal arrows) showing mid-range responses.

when driven by endogenous glutamate release from cone bipolar cells as well. Finally, endogenous ganglion cell responses are the weakest and most diverse, consistent with the idea their serial light-activated \rightarrow glutamate-gated currents may reflect presynaptic integration at the level of bipolar cell terminals. We view this as a major tool for parsing endogenous responses in entire populations.

3.5. Combining excitation mapping with macromolecule immunocytochemistry

A major limitation in the use of excitation mapping has been the strong dependence of AGB trapping on glutaraldehyde, which prevents the use of antibodies against a range of interesting macromolecules that serve as useful classifiers of neurons (Haverkamp & Wässle, 2000). Kalloniatis and colleagues have developed protocols that enable the use of AGB with such probes (see Section 2). Mouse retinas incubated 5 min in Edwards medium (Edwards et al., 1989) with 25 mM AGB were activated with KA or NMDA and the colocalization of activation mapped onto calretinin+ or calbindin+

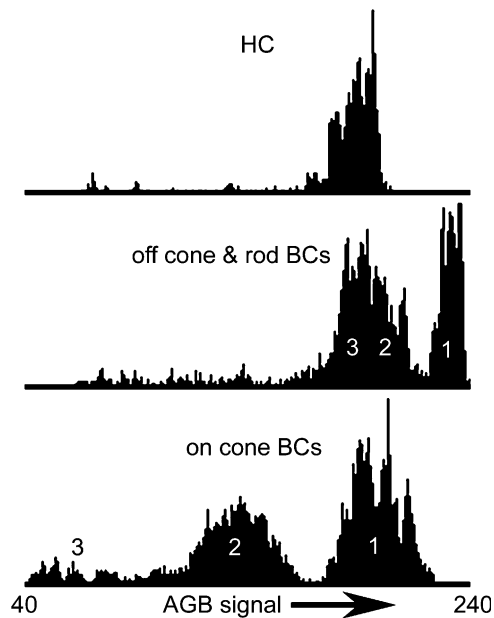


Fig. 10. Three histograms of cellular light-driven responses determined by AGB mapping. The ordinate is the probability density of finding a response at a given AGB signal (abscissa) based on an 8-bit intensity scale (0–255), truncated to a 40–240 grey level range. Cells with a value of 40 are at a “background” signal equivalent to the Müller cell signal. Cells above 40 and approaching 240 represent a range of increasingly stronger responses to the stimulus. The data were derived from Fig. 9. Top: type B HCs show good responses to 550 nm light, but are weaker than some OFF and ON bipolar cells. Middle: the OFF and rod bipolar responses cannot be separated (modes 2 and 3), but subpopulations can be identified, including a highly responsive group (mode 1). Bottom: cone-driven ON bipolar cells are the most distinctive, segregating into at least three major cohorts: poorly responsive (mode 3), moderately responsive (mode 2) and highly responsive (mode 1).

704 neurons by double-label immunocytochemistry
 705 (Fig. 11). While the fine-scale differential responses of
 706 individual neurons cannot be analyzed properly in such
 707 thick sections due to superposition of signals, selective
 708 activation can be achieved. For example, at 5 μM KA,
 709 OFF bipolar cells and some sets of amacrine cells and
 710 ganglion cells are readily detected (Fig. 11A), but this
 711 dose is below threshold for horizontal cells (Marc,
 712 1999b). Several classes of calretinin+ amacrine cells
 713 (red channel) are present, but they have rather weak
 714 responses to KA. Increasing the KA dose to 50 μM gen-
 715 erates robust signals that superimpose nicely on calbin-
 716 din+ horizontal cell somas as a bright orange-yellow
 717 summed signal. Finally, NMDA selectively activates
 718 neurons of the proximal retina (Kalloniatis et al.,
 719 2004; Marc, 1999a, 1999b; Sun et al., 2003), and calbin-
 720 din+ horizontal cells lack any AGB signal, while the cal-
 721 bindin+ amacrine cell cohort is strongly activated by
 722 NMDA. This improved immunocytochemical protocol
 723 offers the opportunity to explore AGB signaling with a
 724 number of new probes.

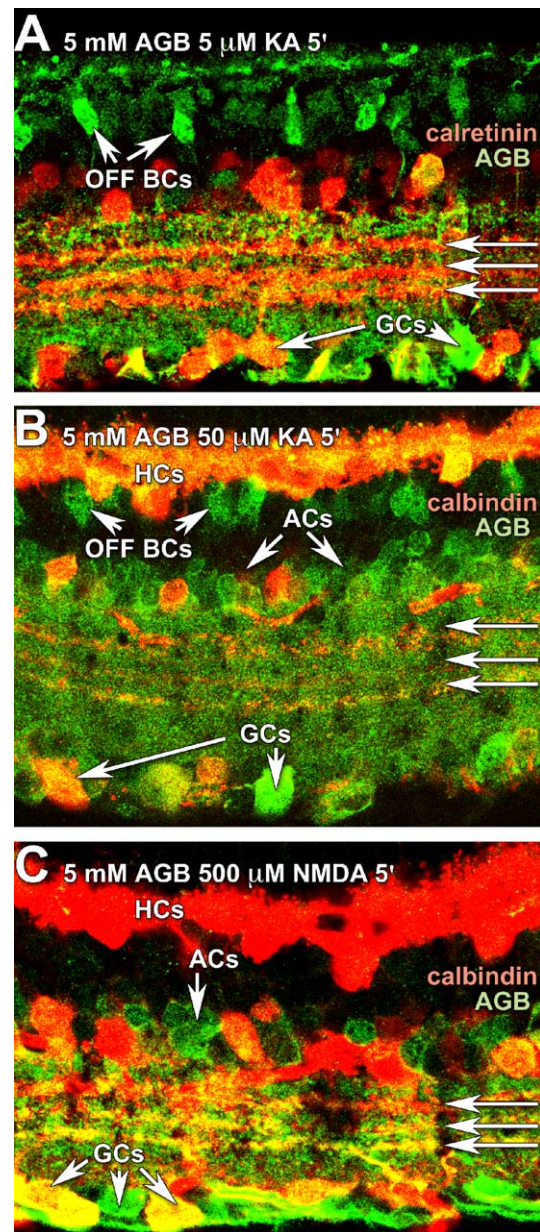


Fig. 11. Concurrent visualization of calcium binding proteins and iGluR signaling using the Kalloniatis method (see text). In each panel, fluorescent imaging maps a calcium binding protein as the red channel and ligand-induced AGB signals as the green channel. (A) Mouse retina incubated in 5 mM AGB + 5 μM KA for 5 min, resulting in strong activation of OFF bipolar cells and amacrine and ganglion cell neurites throughout the IPL. Neurons projecting to a characteristic triple band of ganglion cell rich neurites (see Wässle, 2004) are labeled with anti-calretinin IgGs and visualized with Alexa conjugated secondary IgGs (Molecular Probes). (B) Increasing the KA level to 50 μM recruits horizontal cells (yellow + red signal) into the response spectrum along with OFF bipolar cells and most amacrine and ganglion cells. The horizontal cells are labeled with anti-calbindin IgGs and visualized with Alexa conjugated secondary IgGs. (C) Switching to 500 μM NMDA selectively activates amacrine and ganglion cell subsets, especially (but not exclusively) those that project to the ganglion cell rich triplet bands. Horizontal cells are not activated. The horizontal cells are labeled with anti-calbindin IgGs and visualized with Alexa conjugated secondary IgGs.

725 **4. Discussion**

726 Excitation mapping offers new opportunities to as-
 727 say the behaviors of populations of neurons and retinal
 728 neurons in particular. We have yet to thoroughly ex-
 729 plore all of the applications of the method, but we
 730 are certain that it is a useful tool for analyzing phar-
 731 macologic data, and may even serve as a screening
 732 method for drug leads. The ability to detect both li-
 733 gand-activated and synaptically modulated signaling
 734 offers tremendous opportunities to dissect pathways
 735 and characterize the fundamental signaling attributes
 736 of complex populations of neurons (Kalloniatis et al.,
 737 2004; Marc, 1999a, 1999b; Marc & Jones, 2002; Rohrer
 738 et al., 2004). We now know that all glutamate-driven
 739 cells, including ON bipolar cells, possess channels per-
 740 meant to AGB. In particular, the endogenous AGB
 741 permeation of ON bipolar cells requires the participa-
 742 tion of an AP4-sensitive mechanism, arguing that the
 743 mGluR6 transduction pathway is being probed (Kallo-
 744 niatis et al., 2004). Future applications of AGB map-
 745 ping include screening the emergence of functional
 746 pathways in development and tracking the disassembly
 747 of retinal signaling in disease (Marc, Jones, Watt, &
 748 Strettoi, 2003).

749 We have successfully used intravitreal AGB injec-
 750 tions in fishes, rabbits, and rodents to map endogenous
 751 activity and the patterns are consistent with summed
 752 iGluR and mGluR6 mediated signaling, but these
 753 unpublished data are beyond the scope of this review.
 754 Even so, it is clear that it will also be possible to track
 755 endogenous activity under controlled lighting condi-
 756 tions, in genetic models of function or disease, and un-
 757 der systemic drug treatments. We also know that AGB
 758 mapping reports iGluR signaling in hippocampal slices
 759 (Takahashi, Jones, & Marc, 2004), zebrafish central
 760 pathways (Edwards & Michel, 2002, 2003; Sakata
 761 et al., 2003) and olfactory cell transduction (Lipschitz
 762 & Michel, 2002; Steullet, Cate, Michel, & Derby,
 763 2000). Combined with new evidence that AGB is par-
 764 tially permeant to the blood–brain barrier (Piletz,
 765 May, Wang, & Zhu, 2003), this offers the likelihood
 766 that in vivo CNS excitation mapping can also be
 767 achieved in the short-term.

768 More concretely, we here show that the excitation
 769 mapping method has great latitude; that, as expected
 770 of a channel-mediated process, time and concentra-
 771 tion can be interchanged. Increasing AGB concentra-
 772 tion confers greater sensitivity and large signals
 773 are generated more rapidly. Finally, by varying
 774 some key experimental parameters, it is now possible
 775 to superimpose excitation histories characteristic
 776 of selective AMPA or NMDA channel activation
 777 on structural maps acquired by conventional macro-
 778 molecule immunocytochemistry and fluorescence
 779 detection.

Acknowledgments

This work was supported by NEI Grants EY002576
 and EY015128 (RM), Research to Prevent Blindness
 funding to the University of Utah, and a grant from
 the Health Research Council of New Zealand 02/226
 (MK). MK holds a professorship funded, in part, by
 the Robert G. Leidl estate. Conflict-of-Interest: R.M. is
 a principal of Signature Immunologics.

References

- Balasubramanian, S., Lynch, J. W., & Barry, P. H. (1995). The
 permeation of organic cations through cAMP-gated channels in
 mammalian olfactory receptor neurons. *Journal of Membrane
 Biology*, *146*, 177–191. 789–790
- Chen, B. X., Wilson, S. R., Das, M., Coughlin, D. J., & Erlanger, B. F.
 (1998). Immunology antigenicity of fullerenes: Antibodies specific
 for fullerenes and their characteristics. *Proceedings of the National
 Academy of Sciences of the United States of America*, *95*,
 10809–10813. 791–792
- Datta, S. N., & Iyengar, S. S. (1991). Semi-empirical Hartree-Fock
 calculations on the mechanism of enniatin B mediated transport of
 sodium ions. *Chemistry and Physics Letters*, *183*, 491–498. 793–794
- Dwyer, T. M., Adams, D. J., & Hille, B. (1980). The permeability of
 the endplate channel to organic cations in frog muscle. *Journal of
 General Physiology*, *75*, 469–492. 795–796
- Edwards, F. A., Konnerth, A., Sakmann, B., & Takahashi, T. (1989).
 A thin slice preparation for patch clamp recordings from neurones
 of the mammalian central nervous system. *Plugers Archives*, *414*,
 600–612. 797–798
- Edwards, J. G., & Michel, W. C. (2002). Odor-stimulated glutamatergic
 neurotransmission in the zebrafish olfactory bulb. *Journal of
 Comparative Neurology*, *454*, 294–309. 799–800
- Edwards, J. G., & Michel, W. C. (2003). Pharmacological character-
 ization of ionotropic glutamate receptors in the zebrafish olfactory
 bulb. *Neuroscience*, *122*, 1037–1047. 801–802
- Fairbanks, C. A., Schreiber, K. L., Brewer, K. L., Yu, C.-G., Stone, L.
 S., Kitto, K. F., Nguyen, H. O., Grocholski, B. M., Shoeman, D.
 W., Kehl, L. J., & Regunathan, S. (2000). Agmatine reverses pain
 induced by inflammation, neuropathy, and spinal cord injury.
*Proceedings of the National Academy of Sciences of the United
 States of America*, *97*, 10584–10589. 803–804
- Fambrough, D. M., & Hartzell, H. C. (1972). Acetylcholine receptors:
 number and distribution at neuromuscular junctions in rat
 diaphragm. *Science*, *176*, 189–191. 805–806
- Feng, Y.-Z., Piletz, J. Z., & LeBlanc, M. H. (2002). Agmatine
 suppresses nitric oxide production and attenuates hypoxic-ischemic
 brain injury in neonatal rats. *Pediatric Research*, *52*, 606–611. 807–808
- Galea, E., Regunathan, S., Eliopoulos, V., Feinstein, D. L., & Reis, D.
 J. (1996). Inhibition of mammalian nitric oxide synthase by
 agmatine, an endogenous polyamine formed by decarboxylation
 of arginine. *Biochemistry Journal*, *316*, 247–249. 809–810
- Gründemann, D., Hahne, C., Berkels, R., & Schömig, E. (2003).
 Agmatine is efficiently transported by non-neuronal monoamine
 transporters extraneuronal monoamine transporter (EMT) and
 organic cation transporter 2 (OCT2). *The Journal of Pharmacology
 and Experimental Therapeutics*, *304*, 810–817. 811–812
- Haverkamp, S., & Wässle, H. (2000). Immunocytochemical Anal-
 ysis of the Mouse Retina. *Journal of Comparative Neurology*,
424, 1–23. 813–814
- Hille, B. (2001). *Ion channels of excitable membranes* (3rd ed.).
 Sunderland, MA: Sinauer, p. 722. 815–816

780

788

789

790

791

792

793

794

795

796

797

798

799

800

801

802

803

804

805

806

807

808

809

810

811

812

813

814

815

816

817

818

819

820

821

822

823

824

825

826

827

828

829

830

831

832

833

834

835

836

837

838

839

- 840 Izhaky, D., & Pecht, I. (1998). What else can the immune system
841 recognize? *Proceedings of the National Academy of Sciences of the*
842 *United States of America*, 95, 11509–11510.
- 843 Kalloniatis, M., & Fletcher, E. L. (1993). Immunocytochemical
844 localization of the amino acid neurotransmitters in the chicken
845 retina. *Journal of Comparative Neurology*, 336(2), 174–193.
- 846 Kalloniatis, M., Marc, R. E., & Murry, R. F. (1996). Amino acid
847 signatures in the primate retina. *Journal of Neuroscience*, 16(21),
848 6807–6829.
- 849 Kalloniatis, M., Sun, D., Foster, L., Haverkamp, S., & Wässle, H.
850 (2004). Localization of NMDA receptor subunits and mapping
851 NMDA drive within the mammalian retina. *Visual Neuroscience*,
852 21, 587–597.
- 853 Kunkel, D. D., Lee, L. K., & Stollberg, J. (2001). Ultrastructure of
854 acetylcholine receptor aggregates parallels mechanisms of aggrega-
855 tion. *BMC Neuroscience*(5). doi:10.1186/1471-2202-1182-1119.
- 856 Landsteiner, K. (1945). In *The specificity of serological reactions*
857 (pp. 450). Boston: Harvard University Press.
- 858 Larramendi, L. M., Lorente de No, R., & Vidal, F. (1956). Restoration
859 of sodium-deficient frog nerve fibres by an isotonic solution of
860 guanidinium chloride. *Nature*, 178, 316–317.
- 861 Lipschitz, D. L., & Michel, W. C. (2002). Amino acid odorants
862 stimulate microvillar sensory neurons. *Chemical Senses*, 27,
863 277–286.
- 864 Marc, R. E. (1999a). Kainate activation of horizontal, bipolar,
865 amacrine, and ganglion cells in the rabbit retina. *Journal of*
866 *Comparative Neurology*, 407(1), 65–76.
- 867 Marc, R. E. (1999b). Mapping glutamatergic drive in the vertebrate
868 retina with a channel-permeant organic cation. *Journal of Com-*
869 *parative Neurology*, 407(1), 47–64.
- 870 Marc, R. E., & Cameron, D. A. (2002). A molecular phenotype atlas of
871 the zebrafish retina. *Journal of Neurocytology*, 30, 593–654.
- 872 Marc, R. E., & Jones, B. W. (2002). Molecular phenotyping of retinal
873 ganglion cells. *Journal of Neuroscience*, 22, 412–427.
- 874 Marc, R. E., Jones, B. W., Watt, C. B., & Strettoi, E. (2003). Neural
875 remodeling in retinal degeneration. *Progress in Retinal and Eye*
876 *Research*, 22, 607–655.
- 877 Marc, R. E., Liu, W. L., Kalloniatis, M., Raiguel, S. F., & van
878 Haesendonck, E. (1990). Patterns of glutamate immunoreactivity
879 in the goldfish retina. *Journal of Neuroscience*, 10(12), 4006–4034.
- 880 Marc, R. E., Murry, R. F., & Basinger, S. F. (1995). Pattern
881 recognition of amino acid signatures in retinal neurons. *Journal of*
882 *Neuroscience*, 15(7 Pt. 2), 5106–5129.
- 883 Or, E., David, P., Alla Shainskaya, S., Tal, D. M., & Karlshis, S. J. D.
884 (1993). Effects of competitive sodium-like antagonists on Na,K-
885 ATPase suggest that cation occlusion from the cytoplasmic surface
886 occurs in two steps. *Journal Biological Chemistry*, 268, 16929–16937.
- 887 Pang, J. J., Gao, F., & Wu, S. M. (2004). Light-evoked current
888 responses in rod bipolar cells, cone depolarizing bipolar cells and
All amacrine cells in dark adapted mouse retina. *Journal of* 889
Physiology, 558, 897–912. 890
- Petrunkina, A. M., Harrison, R. A. P., Ekhlesi-Hundrieser, M., & 891
Töpfer-Petersen, E. (2004). Role of volume-stimulated osmolyte 892
and anion channels in volume regulation by mammalian sperm. 893
Molecular and Human Reproduction, 10, 815–823. 894
- Piletz, J. E., May, P. J., Wang, G., & Zhu, H. (2003). Agmatine crosses 895
the blood–brain barrier. *Annals of New York Academy Sciences*, 896
1009, 64–74. 897
- Raasch, W., Schafer, U., Chun, J., & Dominiak, P. (2001). Biological 898
significance of agmatine, an endogenous ligand at imidazoline 899
binding sites. *British Journal of Pharmacology*, 133, 755–780. 900
- Rohrer, B., Blanco, R., Marc, R. E., Lloyd, M. B., Bok, D., 901
Schneeweis, D., et al. (2004). Functionally intact glutamate-med- 902
iated signaling in bipolar-cells of the Trkb knockout mouse retina. 903
Visual Neuroscience, 21, 703–713. 904
- Sakata, Y., Olson, J. K., & Michel, W. C. (2003). Assessment of 905
neuronal maturation and acquisition of functional competence in 906
the developing zebrafish olfactory system. *Methods in Cell Science*, 907
25, 39–48. 908
- Sokoloff, L., Reivich, M., Kennedy, C., Des Rosiers, M. H., Patlak, C. 909
S., Pettigrew, K. D., et al. (1977). The [14C]deoxyglucose method 910
for the measurement of local cerebral glucose utilization: theory, 911
procedure, and normal values in the conscious and anesthetized 912
albino rat. *Journal of Neurochemistry*, 28, 897–916. 913
- Steulet, P., Cate, H. S., Michel, W. C., & Derby, C. D. (2000). 914
Functional units of a compound nose: aesthetasc sensilla house 915
similar populations of olfactory receptor neurons on the crustacean 916
antennule. *The Journal of Comparative Neurology*, 418, 270–280. 917
- Sun, D., Rait, J. L., & Kalloniatis, M. (2003). Inner retinal neurons 918
display differential responses to N-methyl-D-aspartate receptor 919
activation. *The Journal of Comparative Neurology*, 465, 38–56. 920
- Takahashi, D. K., Jones, B. W., Marc, R. E., & K., W. (2004). 921
Excitation mapping in a rodent seizure model. *American Epilepsy*
Society, 58th Annual Meeting, Abstract 1.040. 922
923
- Tasaki, I., Watanabe, A., & Singer, I. (1966). Excitability of squid 924
giant axons in the absence of univalent cations in the external 925
medium. *Proceedings of the National Academy of Sciences of the*
United States of America, 56, 1116–1122. 926
927
- Weininger, D., Weininger, A., & J.L., W. (1989). SMILES. 2. 928
Algorithm for generation of unique SMILES notation. *Journal of*
Chemical Information and Computer Science, 29, 97–101. 929
930
- Yingcharoen, K., Rinvik, E., Storm-Mathisen, J., & Ottersen, O. P. 931
(1989). Gaba, glycine, glutamate, aspartate and taurine in the 932
perihypoglossal nuclei—an immunocytochemical investigation in 933
the cat with particular reference to the issue of amino-acid 934
colocalization. *Experimental Brain Research*, 78(2), 345–357. 935
- Yoshikami, D. (1981). Transmitter sensitivity of neurons assayed by 936
autoradiography. *Science*, 212, 929–930. 937
938

insert: □

Waessle, H. (2004) Parallel processing in the mammalian retina. *Nature Reviews Neuroscience* 5, 1-11. □